INTERNATIONAL JOURNAL FOR NUMERICAL METHODS IN ENGINEERING
Int. J. Numer. Meth. Engng 2006; **65**:2060–2090
Published online 26 October 2005 in Wiley InterScience (www.interscience.wiley.com). DOI: 10.1002/nme.1536

Radial basis functions and level set method for structural topology optimization

Shengyin Wang[‡] and Michael Yu Wang[*, †]

Department of Automation and Computer-Aided Engineering, The Chinese University of Hong Kong, Shatin, NT, Hong Kong

SUMMARY

Level set methods have become an attractive design tool in shape and topology optimization for obtaining lighter and more efficient structures. In this paper, the popular radial basis functions (RBFs) in scattered data fitting and function approximation are incorporated into the conventional level set methods to construct a more efficient approach for structural topology optimization. RBF implicit modelling with multiquadric (MQ) splines is developed to define the implicit level set function with a high level of accuracy and smoothness. A RBF–level set optimization method is proposed to transform the Hamilton–Jacobi partial differential equation (PDE) into a system of ordinary differential equations (ODEs) over the entire design domain by using a collocation formulation of the method of lines. With the mathematical convenience, the original time dependent initial value problem is changed to an interpolation problem for the initial values of the generalized expansion coefficients. A physically meaningful and efficient extension velocity method is presented to avoid possible problems without reinitialization in the level set methods. The proposed method is implemented in the framework of minimum compliance design that has been extensively studied in topology optimization and its efficiency and accuracy over the conventional level set methods are highlighted. Numerical examples show the success of the present RBF–level set method in the accuracy, convergence speed and insensitivity to initial designs in topology optimization of two-dimensional (2D) structures. It is suggested that the introduction of the radial basis functions to the level set methods can be promising in structural topology optimization. Copyright © 2005 John Wiley & Sons, Ltd.

KEY WORDS: topology optimization; radial basis functions; level set method; extension velocity; conceptual design

*Correspondence to: Michael Yu Wang, Department of Automation and Computer-Aided Engineering, The Chinese University of Hong Kong, Shatin, NT, Hong Kong.
†E-mail: yuwang@acae.cuhk.edu.hk
‡E-mail: sywang@acae.cuhk.edu.hk

Contract/grant sponsor: Research Grants Council of Hong Kong SAR; contract/grant number: CUHK4164/03E
Contract/grant sponsor: Chinese University of Hong Kong; contract/grant number: 04/ENG1
Contract/grant sponsor: Natural Science Foundation of China; contract/grant numbers: 50128503; 50390063

Received 1 June 2005
Revised 1 September 2005
Accepted 1 September 2005

1. INTRODUCTION

Structural optimization problems would include shape, sizing and topology optimization. It has been generally regarded that structural topology optimization is one of the most important structural optimization methods because of its ability in achieving greatest savings [1–3]. However, structural topology optimization has also been identified as one of the most challenging tasks in structural design.

The finite element (FE) based structural topology optimization as a generalized shape optimization problem has received wide attention and experienced considerable progress recently [4–16], as reviewed in detail in References [1, 17, 18]. A wide range of approaches and techniques has been developed [2, 4, 18–21] since the seminal work of Bendsøe and Kikuchi [2]. As reviewed by many researchers [1, 17, 22, 23], one of the most established families of methods is the one based on the homogenization approach first proposed by Bendsøe and Kikuchi [2], in which the structural form is represented by microstructures with voids and the material throughout the structure is redistributed by using an optimality criteria procedure. As an important alternative approach, the power-law approach [24], which is also called the solid isotropic microstructure with penalization (SIMP) method [25] and originally introduced by Bendsøe [19], has got a fairly general acceptance in recent years [1] because of its computational efficiency and conceptual simplicity. In the SIMP method, the material properties can be expressed in terms of the design variable material density using a simple 'power-law' interpolation as an explicit means to suppress intermediate values of the bulk density. However, SIMP does not directly resolve the problem of non-existence of solutions (ill-posedness) [18] and thus numerical insatiabilities may occur [16]. Another recognized family of structural optimization methods is the one based on the evolutionary structural optimization (ESO) approach proposed by Xie and Steven [3], in which the material in a design domain which is not structurally active is considered as inefficiently used and can thus be slowly removed [26]. These families of topology optimization methods have been further developed by a large number of researchers [1, 23, 27].

For structural shape and topology optimization problems, an emerging family of methods is the one based on the implicit moving interfaces using the level set methods [10, 11, 28, 29]. The level set method introduced by Osher and Sethian [30] is a simple and versatile method for computing and analysing the motion of an interface in two or three dimensions and following the evolution of interfaces. Since these interfaces may easily develop sharp corners, break apart, and merge together, the level set method has a wide range of applications, including problems in fluid mechanics, combustion, solids modelling, computer animation and image processing [31].

Sethian and Wiegmann [28] are among the first researchers to extend the level set method of Osher and Sethian to capture the free boundary of a structure on a fixed Eulerian mesh and the Von Mises equivalent stress was used to improve the structural rigidity. Osher and Santosa [32] investigated a two-phase optimization of a membrane modelled by a linear scalar partial differential equation. The level set method was combined with the shape sensitivity analysis framework, but without the context of linear or non-linear elasticity. Wang *et al.* [10] established the speed vector in terms of the shape of the boundary and the variation sensitivity as a meaningful link between the general structural optimization process and the powerful level set method. It is also shown that using the level set method for structural topology optimization has the promising potential in the flexibility of handling topological changes, fidelity of boundary representation and degree of automation. The level set methods are further

developed as a natural setting to combine the rigorous shape variations into the conventional optimization process in Reference [29]. Allaire *et al.* [11] proposed a similar implementation of the level set method where the front velocity during the optimization process is derived from a strict shape sensitivity analysis by using an adjoint problem and the front propagation is performed by solving a Hamilton–Jacobi equation. Furthermore, drastic topology changes during the optimization process were allowed for. Different from the conventional level set methods, Belytschko *et al.* [8] developed an implicit function regularization method, in which the Heaviside step function is regularized to permit the evaluation of sensitivities. However, low order approximations such as C^0 shape functions in Reference [8] can only ensure that the implicit function, rather than its partial derivatives, to be continuous across meshes. Hence, the mesh size must be sufficiently fine and the computational cost may thus become formidable. It should be noted that a recent result in Reference [33] has shown that the most common technique for the regularization of the Dirac delta function in level set methods is inconsistent, and may lead to $\mathcal{O}(1)$ errors. More recently, the level set method was further extended to a level set-based variational approach for the design of heterogeneous objects using a multi-phase level set model in Reference [34], in which the promising features such as strong regularity in the problem formulation and inherent capabilities of geometric and materials modelling have been obtained and illustrated.

In practice, in applying a level set method for structural topology optimization, it should be noted that the implementation of the conventional discrete level set methods requires appropriate choice of the upwind schemes, extension velocities and reinitialization algorithms. In general, it is well known that the PDEs are rarely easy to implement [35], though some robust and accurate upwind schemes have been presented [30, 36, 37]. Furthermore, there is no nucleation mechanism in the conventional level set method, if the Hamilton–Jacobi equation is solved under a strict condition for numerical stability [38, 39]. Indeed, new holes cannot be created in the interior of a material region because the Hamilton–Jacobi equation satisfies a maximum principle and reinitialization must be applied to the level set function to ensure its regularity [39, 40]. Although some attempts have been made to incorporate both the topological derivatives and the shape derivatives into the level set methods to resolve this problem [39, 40], it is shown to be difficult to switch between the topological derivatives and the shape derivatives [40–42] and to handle surface functions [43]. Hence, the numerical considerations of discrete computation have severely limited the primary advantages of the level set methods in solid optimization.

The objective of this study is to present an effective level set method for structural topology optimization based on the popular radial basis functions (RBFs) in scattered data fitting and function approximation [44, 45]. The implicit level set function is approximated by using the RBF implicit modelling with multiquadric (MQ) splines to achieve a high level of accuracy and smoothness [45]. By assuming that the time dependence of the implicit function is due to the generalized expansion coefficients of the RBF interpolant, the Hamilton–Jacobi PDE is converted into a mathematically more convenient ODE and the original time dependent initial value problem is changed to an interpolation problem for the initial values of the generalized expansion coefficients. A collocation formulation of the method of lines is further derived by assuming the finite element nodes as the RBF knots. Furthermore, a physically meaningful and efficient extension velocity method is presented and potential problems without reinitialization in the level set methods can be alleviated. This proposed RBF–level set method is implemented in the framework of topological optimum of minimum compliance design that has been extensively

studied in topology optimization and its efficiency and accuracy over the conventional level set methods are highlighted. Numerical examples are chosen to illustrate the success of the present method in accuracy, convergence speed and insensitivity to initial designs in topology optimization of 2D structures.

In the following, we first present an overview on the level set-based topology optimization for minimum compliance design. We then introduce the RBF implicit modelling for the implicit level set function. Properties of the RBF MQ splines as well as the implementation of the implicit modelling are discussed and formulated. A RBF–level set optimization is then proposed. Numerical examples are discussed next with a comparative study and the efficiency and accuracy of the present method are highlighted. The conclusions are finally given.

2. RBF–LEVEL SET METHOD FOR TOPOLOGY OPTIMIZATION

2.1. Level set-based topology optimization

Level set methods first introduced by Osher and Sethian [30] have become popular recently for tracking, modelling and simulating the motion of dynamic interfaces (free boundaries) in fluid mechanics, combustion, computer animation and image processing [31]. These interfaces can develop sharp corners, break apart, and merge together automatically. The surface is represented implicitly through a level set function $\Phi(\mathbf{x})$, which is Lipschitz-continuous, and the surface itself is the zero isosurface or zero level set $\{\mathbf{x} \in \mathbb{R}^d \mid \Phi(\mathbf{x}) = 0\}$ ($d = 2$ or 3). Furthermore, the surface motion can be described by PDEs involving $\Phi(\mathbf{x})$. In the present level set-based shape and topology optimization method, the shape and topology of a structure are described by a level set function $\Phi(\mathbf{x})$ defined as

$$\begin{aligned} \Phi(\mathbf{x}) &= 0 \quad \forall \mathbf{x} \in \partial\Omega \cap D \\ \Phi(\mathbf{x}) &< 0 \quad \forall \mathbf{x} \in \Omega \backslash \partial\Omega \\ \Phi(\mathbf{x}) &> 0 \quad \forall \mathbf{x} \in (D \backslash \Omega) \end{aligned} \tag{1}$$

where $D \subset \mathbb{R}^d$ is a fixed design domain in which all admissible shapes Ω (a smooth bounded open set) are included, i.e. $\Omega \subset D$. Figure 1 illustrates this implicit representation of the shape of a 2×1 plate with a central hole, in which the boundary of the central hole is represented by $\Phi(x) = 0$.

In the level set-based topology optimization methods [10, 11], the structural topology optimization process operates on the implicit scalar function $\Phi(\mathbf{x})$ defined in Equation (1) and uses a gradient method for the minimization of an objective function $J(\Phi)$. In the present study, only a relatively simple unconstrained optimal topology design problem presented in Reference [11] with a design-independent load is considered, which can be expressed as

$$\min_{\Phi(\mathbf{x})}: J(\Phi) = \int_D (\boldsymbol{\varepsilon}(\mathbf{u}))^{\mathrm{T}} \mathbf{C} \boldsymbol{\varepsilon}(\mathbf{u}) H(-\Phi)\, \mathrm{d}\Omega + \ell \int_D H(-\Phi)\, \mathrm{d}\Omega \tag{2}$$

where $\mathbf{u}$ is the displacement field, $\boldsymbol{\varepsilon}(\mathbf{u})$ the strain field, $H(\Phi)$ the Heaviside step function of the implicit function $\Phi(\mathbf{x})$ [35], ℓ a positive Lagrange multiplier, and the volume V of

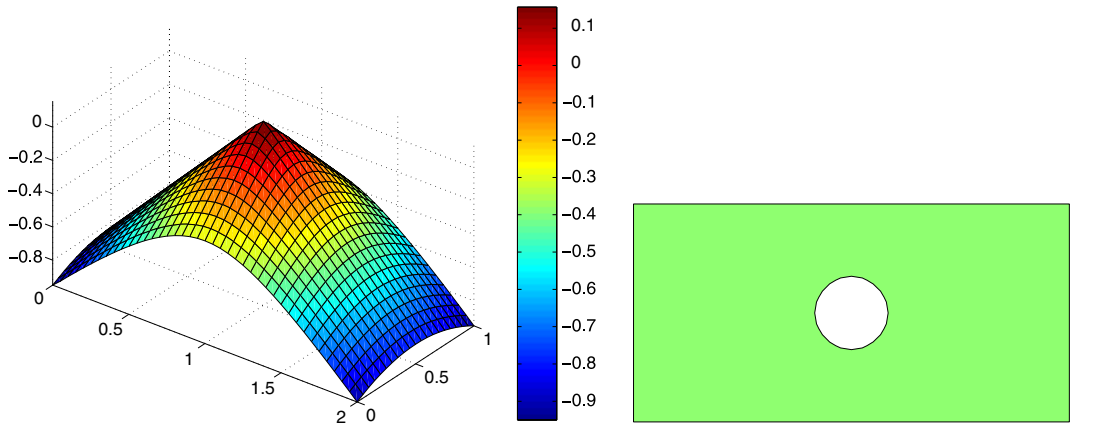

Figure 1. Implicit representation of a 2×1 plate with a central hole: (a) implicit function $\Phi(\mathbf{x})$; and (b) the corresponding design.

the admissible design can be written as

$$V = \int_D H(-\Phi)\,\mathrm{d}\Omega \tag{3}$$

It should be noted that, different from the standard minimum compliance optimization problem [18], the value of the Lagrange multiplier ℓ in Equation (2) is here explicitly prescribed, and the corresponding optimal topology design problem is simplified as a computationally more efficient unconstrained optimization problem without any explicitly defined volume constraint, as shown in the work of Allaire *et al.* [11]. On the other hand, if a volume constraint is to be strictly applied to the minimum compliance design problem, as done in the classical minimum compliance design problems using the SIMP method in the literature [16, 18, 24, 46], the value of ℓ should be variable during the optimization process. Further study on this relatively more complicated case has been included in another work of the authors [47] and is out of the interest of the present study.

Based on local perturbations of the boundary of the admissible domain Ω, the resulting shape derivative [11] of the objective function $J(\Phi)$ can be written as

$$\frac{\mathrm{d}J}{\mathrm{d}t} = -\int_{\partial\Omega} ((\boldsymbol{\varepsilon}(\mathbf{u}))^{\mathrm{T}}\mathbf{C}\boldsymbol{\varepsilon}(\mathbf{u}) - \ell)v_n\,\mathrm{d}s \tag{4}$$

where t is the artificial time, and v_n the artificial normal velocity. According to Equation (4), a descent direction of the normal velocity v_n can be defined as

$$v_n = (\boldsymbol{\varepsilon}(\mathbf{u}))^{\mathrm{T}}\mathbf{C}\boldsymbol{\varepsilon}(\mathbf{u}) - \ell \tag{5}$$

in which the normal velocity v_n on the boundary of the shape is related with the strain energy density. It should be noted that since a fixed grid is used in the present Eulerian-type approach, the normal velocity v_n must be extended either to the whole design domain D [11] or to a narrow band [31]. Moreover, the choice of extension velocities can directly influence the overall

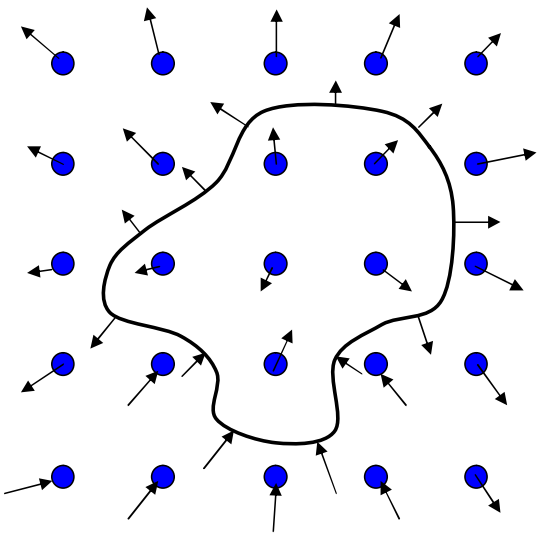

Figure 2. An extension velocity field for the level set method with a fixed grid.

efficiency [48]. Figure 2 demonstrates an extension velocity field, in which the normal velocities at the front (zero level set or free boundary) are extended to each grid point in the design domain, and the discontinuity of the velocity field across the front is almost eliminated.

In the level set-based topology optimization, the normal velocity v_n is used as the advection velocity in the following Hamilton–Jacobi equation [30, 31, 49]:

$$\frac{\partial \Phi}{\partial t} + v_n |\nabla \Phi| = 0 \tag{6}$$

Hence, moving the boundary of the shape ($\Phi(\mathbf{x}) = 0$) along the descent gradient direction is equivalent to transporting Φ by solving the Hamilton–Jacobi equation (6). Usually, the robust upwind schemes [30, 36, 37] can be used to solve this equation accurately. In the conventional level set methods, since the solution of Equation (6) often becomes very flat and/or steep at the front [50], a reinitialization procedure is needed to resurrect the behaviour of $\Phi(\mathbf{x})$ in the neighbourhood of the front. Reinitialization is usually applied as an auxiliary step, but it is very important to guarantee a good approximation of the normal n or the curvature of the boundary.

2.2. Limitations of discrete level set method

In the conventional level set-based topology optimization, a general analytical function for $\Phi(t, \mathbf{x})$ is not known. Thus, it must be discretized for level set processing, often through a distance transform. In an Eulerian approach, a numerical procedure for solving the Hamilton–Jacobi PDE is indispensable. This procedure requires an appropriate choice of the upwind schemes, extension velocities and reinitialization algorithms, which may limit the utility of the level set method [35]. Some of the limitations are discussed earlier. For example, reinitialization

prevents a level set function from nucleation of holes in the interior of material regions [38, 39]. Another major limitation lies in the discrete representation.

In the Eulerian approach, the transport equation (6) is solved with a finite difference or finite element method over a fixed grid or mesh [10, 11, 28]. Since the grid is fixed in space, only the nodal values of the implicit function $\Phi(\mathbf{x})$ are used directly. One of the key steps in the Eulerian approach is to describe the geometry (or topology) by the nodal values of $\Phi(\mathbf{x})$ and shape functions to ensure that the space of achievable designs will be smooth enough in shape [31, 51]. In practice, only low order approximations such as C^0 shape functions [8, 31, 52] are used because of the polynomial snaking problem [53] that polynomial interpolation in high dimensions can easily lead to singular problems and cause derivative estimates to be very poor [45]. Hence, only the implicit function $\Phi(\mathbf{x})$, rather than its partial derivatives, can be guaranteed to be continuous across meshes. Furthermore, the spatial truncation errors due to the low order schemes can only be controlled by using progressively smaller meshes [8, 10, 11]. Therefore, the mesh spacing must be sufficiently fine to capture the partial derivative behaviour accurately and to avoid numerical artifacts contaminating the solution. This makes the computation quite time and memory consuming.

Therefore, a better method is to retain topological benefits of the implicit representation of a level set model while avoiding the drawbacks of using its discrete samples on a fixed grid or mesh. In the present study, we propose to generalize the level set function $\Phi(t, \mathbf{x})$ to include alternative implicit surface representations which provide a free-form representation with parameterization. To this end, a level set method using radial basis functions (RBFs) is developed for structural topology optimization.

By using RBF interpolation and modelling we can achieve the global smoothness of the implicit function and, thus, significantly improve the accuracy and efficiency of the level set methods. Parameterization of the implicit model will convert the Hamilton–Jacobi PDE into a system of mathematically more convenient ordinary differential equations (ODEs). Moreover, reinitialization becomes unnecessary, which would allow for nucleation of new holes. This proposed method is discussed in detail in the following sections.

2.3. RBF implicit modelling

To model and reconstruct the entire admissible design with a single function which is globally continuous and differentiable, an implicit modelling method based on radial basis functions (RBFs) is presented here. RBFs are popular for interpolating scattered data to produce smooth surface/boundary as the associated system of non-linear equations is guaranteed to be invertible under mild conditions on the locations of the data points [54]. In Reference [44], thorough theoretical and implementation viewpoints on RBFs have been presented and interpolations based on radial basis functions are shown to be effective when the functions to be approximated are of multiple variables, or are given only by a great amount of data or by scattered data. In real-world applications, radial basis function techniques have become extremely useful, ranging from pattern reconstruction, artificial intelligence, to simply solving mathematical PDEs based on irregular data distributions [52]. The positive features of radial basis functions such as the unique solvability of the interpolation problem, the computation of interpolants, their smoothness and convergence make them very attractive in topology optimization. In the present RBF–level set method for topology optimization, RBF implicit modelling is to be presented as an effective representation method to reconstruct the shape and topology of an admissible design.

Table I. Common radial basis functions ($r = r_i = \|\mathbf{x} - \mathbf{x}_i\|$).

Name	$\varphi(r)$	Parameters
Thin-plate spline	$r^2 \ln r$	$\mathbf{x} \in \mathbb{R}^2$
Cubic spline	r^3	$\mathbf{x} \in \mathbb{R}^3$
Polyharmonic splines	$r^{2n} \ln r$	$n \geqslant 1, \mathbf{x} \in \mathbb{R}^2$
Polyharmonic splines	r^{2n-1}	$n \geqslant 1, \mathbf{x} \in \mathbb{R}^3$
Sobolev spline	$r^v K_v(r)$	$v>0$, K_v: spherical Bessel function
Matern spline	$e^{-cr} K_v(cr)$	$v>0, c>0$
Exponential spline	e^{-cr}	$c>0$
Gaussians	e^{-cr^2}	$c>0$
Multiquadrics	$\sqrt{r^2 + c^2}$	$c>0$
Compactly supported	$(1-r)_+^m p(r)$	$m \geqslant 2$, $p(r)$: polynomial of Wendland

Radial basis functions are radially symmetric functions centred at a particular point [55], or knot, which can be expressed as follows:

$$\varphi_i(\mathbf{x}) = \varphi(\|\mathbf{x} - \mathbf{x}_i\|), \quad \mathbf{x}_i \in D \tag{7}$$

where $\|\cdot\|$ denotes the Euclidean norm on $\mathbb{R}^d$ [56], and $\mathbf{x}_i$ the position of the knot. Only a single fixed function form $\varphi : \mathbb{R}^+ \to \mathbb{R}$ with $\varphi(0) \geqslant 0$ is used as the basis to form a family of independent functions. There is a large class of possible radial basis functions. Commonly used RBFs include thin-plate spline, polyharmonic splines, Sobolev splines, Gaussians, multiquadrics and compactly supported RBFs [45, 56], etc., as shown in Table I. Among these common functions, the multiquadric (MQ) spline appears to be the overall best performing RBF, which can be written as

$$\varphi_i(\mathbf{x}) = \sqrt{(\mathbf{x} - \mathbf{x}_i)^2 + c_i^2} \tag{8}$$

where c_i is the free shape parameter which is commonly assumed to be a constant for all i in most applications [56]. Figure 3 displays the MQ splines centred at the original point with two different shape parameters (1 and 0.0001). It can be seen that a larger shape parameter leads to a flatter shape which is less sensitive to the difference in radial distance. It should also be noted that $\varphi_i(\mathbf{x})$ in Equation (8) is continuously differentiable and thus MQ splines are infinitely smooth splines [45]. The physical foundation of MQ splines is that MQ is related to a consistent solution of the biharmonic potential problem, as shown by Hardy [57]. The conditional positive definiteness of the multiquadric collocation matrices has been proven by Micchelli [58]. The exponential convergence of the error of the MQ approximation was demonstrated by Madych and Nelson [59] and Cheng *et al.* [56]. Furthermore, MQ was ranked the best in interpolation for scattered data by Franke [60].

In the present RBF implicit modelling, MQ is used to interpolate the scalar implicit function $\Phi(\mathbf{x})$ with N knots by using N MQs centred at these knots. The resulting RBF interpolant of the implicit function can be written as

$$\Phi(\mathbf{x}) = \sum_{i=1}^{N} \alpha_i \varphi_i(\mathbf{x}) + p(\mathbf{x}) \tag{9}$$

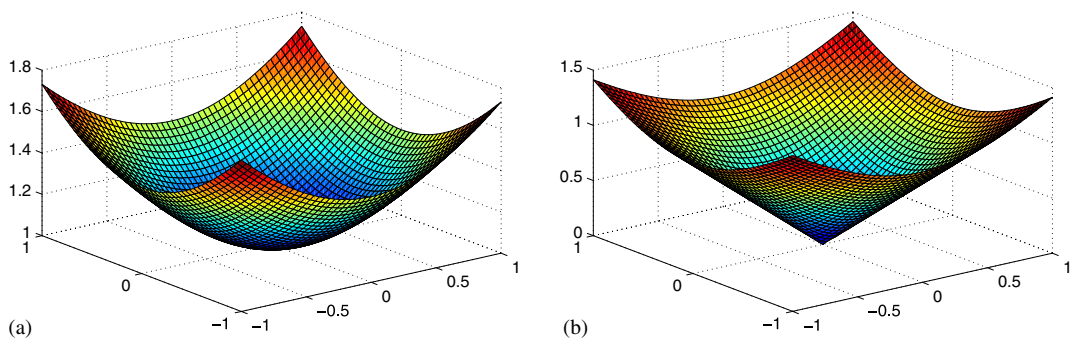

Figure 3. Multiquadric splines: (a) $c = c_i = 1$; and (b) $c = c_i = 0.0001$.

where α_i is the weight, or expansion coefficient, of the radial basis function positioned at the ith knot, $p(\mathbf{x})$ a first-degree polynomial to account for the linear and constant portions of $\Phi(\mathbf{x})$ and to ensure positive definiteness of the solution [55]. For the three-dimensional (3D) modelling problems, $p(\mathbf{x})$ can be given by

$$p(\mathbf{x}) = p_0 + p_1 x + p_2 y + p_3 z \tag{10}$$

in which p_0, p_1, p_2 and p_3 are the coefficients of the polynomial $p(\mathbf{x})$. Because of the introduction of this polynomial, to ensure a unique solution, the RBF interpolant of $\Phi(\mathbf{x})$ in Equation (9) must be subject to the following orthogonality or side constraints [45, 54, 55, 57]:

$$\sum_{i=1}^{N} \alpha_i = 0; \quad \sum_{i=1}^{N} \alpha_i x_i = 0; \quad \sum_{i=1}^{N} \alpha_i y_i = 0; \quad \sum_{i=1}^{N} \alpha_i z_i = 0 \tag{11}$$

If the interpolation data values $f_1, \ldots, f_N \in \mathbb{R}$ at knot locations $\mathbf{x}_1, \ldots, \mathbf{x}_N \in \Omega \subset \mathbb{R}^d$ are given, the RBF interpolant of $\Phi(\mathbf{x})$ in Equation (9) can be obtained by solving the system of $N + 4$ linear equations for $N + 4$ unknown expansion coefficients:

$$\Phi(\mathbf{x}_i) = f_i, \quad i = 1, \ldots, N$$

$$\sum_{i=1}^{N} \alpha_i = 0; \quad \sum_{i=1}^{N} \alpha_i x_i = 0; \quad \sum_{i=1}^{N} \alpha_i y_i = 0; \quad \sum_{i=1}^{N} \alpha_i z_i = 0 \tag{12}$$

which can be rewritten in the matrix form as

$$\mathbf{H}\boldsymbol{\alpha} = \mathbf{f} \tag{13}$$

where

$$\mathbf{H} = \begin{bmatrix} \mathbf{A} & \mathbf{P} \\ \mathbf{P}^{\mathrm{T}} & \mathbf{0} \end{bmatrix} \in \mathbb{R}^{(N+4)\times(N+4)} \tag{14}$$

$$\mathbf{A}=\begin{bmatrix}\varphi_1(\mathbf{x}_1) & \cdots & \varphi_N(\mathbf{x}_1)\\ \vdots & \ddots & \vdots\\ \varphi_1(\mathbf{x}_N) & \cdots & \varphi_N(\mathbf{x}_N)\end{bmatrix}\in\mathbb{R}^{N\times N} \tag{15}$$

$$\mathbf{P}=\begin{bmatrix}1 & x_1 & y_1 & z_1\\ \vdots & \vdots & \vdots & \vdots\\ 1 & x_N & y_N & z_N\end{bmatrix}\in\mathbb{R}^{N\times 4} \tag{16}$$

$$\boldsymbol{\alpha}=[\alpha_1\ \cdots\ \alpha_N\ \ p_0\ \ p_1\ \ p_2\ \ p_3]^{\mathrm{T}}\in\mathbb{R}^{N+4} \tag{17}$$

$$\mathbf{f}=[f_1\ \cdots\ f_N\ \ 0\ \ 0\ \ 0\ \ 0]^{\mathrm{T}}\in\mathbb{R}^{N+4} \tag{18}$$

Since the multiquadric collocation matrix $\mathbf{H}$ is theoretically invertible [44, 45, 48], the generalized expansion coefficients $\boldsymbol{\alpha}$ can be given by

$$\boldsymbol{\alpha}=\mathbf{H}^{-1}\mathbf{f} \tag{19}$$

To solve Equation (13) for relatively simple and small-size problems, it is possible to use LU factorization (an $\mathcal{O}((N+4)^3)$ algorithm) or iterative means in $\mathcal{O}((N+4)^2)$ [55]. However, these methods may become computationally too expensive and even impractical [54] when applied to large-scale and/or 3D problems. Hence, the fast evaluation methods [54] based on the fast multipole method (FMM) [61], which can greatly reduce the storage and computational costs of using RBFs, should be adopted. After obtaining the generalized expansion coefficients $\boldsymbol{\alpha}$, the resulting RBF interpolant of the implicit function in Equation (9) can be re-written compactly as

$$\Phi(\mathbf{x})=\boldsymbol{\phi}^{\mathrm{T}}(\mathbf{x})\boldsymbol{\alpha} \tag{20}$$

where

$$\boldsymbol{\phi}(\mathbf{x})=[\varphi_1(\mathbf{x})\ \cdots\ \varphi_N(\mathbf{x})\ \ 1\ \ x\ \ y\ \ z]^{\mathrm{T}}\in\mathbb{R}^{(N+4)\times 1} \tag{21}$$

2.4. RBF–level set optimization method

A RBF–level set method is proposed to transform the Hamilton–Jacobi PDE into a system of first-order ordinary differential equations (ODEs) over the entire domain D to solve topology optimization problems using the level set methods efficiently with a significant mathematical convenience. As aforementioned, in the level set-based topology optimization methods, moving the boundary of the shape along a descent gradient direction to find an optimal shape and topology is equivalent to transporting the scalar implicit function $\Phi(\mathbf{x})$ by solving the Hamilton–Jacobi equation (6) and thus the optimal propagation of the front is performed by solving the Hamilton–Jacobi PDE [11]. In the present study, RBF implicit modelling is used to interpolate $\Phi(\mathbf{x})$ with N knots by using N MQs centred at these knots. Since the Hamilton–Jacobi equation (6) is time dependent, it is assumed that the space and time are separable and the time dependence of the implicit function Φ is due to the generalized expansion coefficients $\boldsymbol{\alpha}$

of the RBF interpolant in Equation (17). With these assumptions, the RBF interpolant of the implicit function in Equation (20) becomes time dependent as follows:

$$\Phi = \Phi(\mathbf{x}, t) = \boldsymbol{\phi}^{\mathrm{T}}(\mathbf{x})\boldsymbol{\alpha}(t) \tag{22}$$

and the orthogonality constraints in Equation (11) can be re-written as

$$\sum_{i=1}^{N} \alpha_i(t) = 0; \quad \sum_{i=1}^{N} \alpha_i(t) x_i = 0; \quad \sum_{i=1}^{N} \alpha_i(t) y_i = 0; \quad \sum_{i=1}^{N} \alpha_i(t) z_i = 0 \tag{23}$$

Substituting Equation (22) into the Hamilton–Jacobi equation (6) yields

$$\boldsymbol{\phi}^{\mathrm{T}} \frac{\mathrm{d}\boldsymbol{\alpha}}{\mathrm{d}t} + v_n |(\nabla \boldsymbol{\phi})^{\mathrm{T}} \boldsymbol{\alpha}| = 0 \tag{24}$$

where

$$\nabla \boldsymbol{\phi} = \frac{\partial \boldsymbol{\phi}}{\partial x}\mathbf{i} + \frac{\partial \boldsymbol{\phi}}{\partial y}\mathbf{j} + \frac{\partial \boldsymbol{\phi}}{\partial z}\mathbf{k} \tag{25}$$

$$|(\nabla \boldsymbol{\phi})^{\mathrm{T}} \boldsymbol{\alpha}| = \left[\left(\frac{\partial \boldsymbol{\phi}^{\mathrm{T}}}{\partial x} \boldsymbol{\alpha} \right)^2 + \left(\frac{\partial \boldsymbol{\phi}^{\mathrm{T}}}{\partial y} \boldsymbol{\alpha} \right)^2 + \left(\frac{\partial \boldsymbol{\phi}^{\mathrm{T}}}{\partial z} \boldsymbol{\alpha} \right)^2 \right]^{1/2} \tag{26}$$

In Equation (24), the RBF expansion coefficients are explicitly time dependent and all the time dependence is due to the expansion coefficients. At the initial time, all the time dependent variables should be specified over the entire domain. This initial value problem can be considered equivalent to an interpolation problem since the expansion coefficients at the initial time are found as a solution of the interpolation problem, as shown in Equation (13). Hence, the preliminary starting point of the use of RBFs to solve PDEs is the interpolation problem that is equivalent to solving the initial value problem. The original time dependent initial value problem has thus become an interpolation problem for the initial values of the generalized expansion coefficients $\boldsymbol{\alpha}$. To time advance the initial values $\boldsymbol{\alpha}$, a collocation method is introduced. In the present Eulerian type approach, all the nodes of the fixed mesh are taken as the fixed knots of the RBF interpolation for the implicit function $\Phi(\mathbf{x})$. As an extension, Equation (24) is then applied to each of these knots of the RBF interpolation, rather than only the points at the front. The normal velocity v_n in Equation (24) is thus extended as v_n^e to all these knots in the design domain D. This is illustrated in Figure 2, where each of the grid point is considered as a knot of the RBF.

By using this collocation method and the orthogonality constraints in Equation (23), a set of ODEs can be obtained as follows:

$$\mathbf{H} \frac{\mathrm{d}\boldsymbol{\alpha}}{\mathrm{d}t} + \mathbf{B}(\boldsymbol{\alpha}) = 0 \tag{27}$$

where

$$\mathbf{B}(\boldsymbol{\alpha}) = \begin{bmatrix} v_n^e(\mathbf{x}_1)|(\nabla\boldsymbol{\phi}^{\mathrm{T}}(\mathbf{x}_1))\boldsymbol{\alpha}| \\ \vdots \\ v_n^e(\mathbf{x}_N)|(\nabla\boldsymbol{\phi}^{\mathrm{T}}(\mathbf{x}_N))\boldsymbol{\alpha}| \\ 0 \\ 0 \\ 0 \\ 0 \end{bmatrix} \in \mathbb{R}^{(N+4)\times 1} \tag{28}$$

It should be noted that Equation (27) is a collocation formulation of the method of lines [62], in which a PDE problem is reduced to a simpler ODE problem by discretization. The method of lines has a solid mathematical foundation and the convergence of the solution of the converted ODE problem to the solution of the original PDE problem has been rigorously proven [62]. In Equation (28), the spatial derivative $\nabla\boldsymbol{\phi}$ can be found analytically from Equation (21) due to the RBF interpolation.

The set of coupled non-linear ODEs of Equation (27) can be solved by several different ODE solvers such as the first-order forward Euler's method and higher-order Runge–Kutta, Runge–Kutta–Fehlberg, Adams–Bashforth, or Adams–Moulton methods [63]. In the present study, only the first-order forward Euler's method is used since it is the simplest solution algorithm for ODE initial condition problems and often used for comparison with more accurate algorithms, which are more complex and tedious to implement. Using Euler's method, an approximate solution to Equation (27) can be given by

$$\boldsymbol{\alpha}(t^{n+1}) = \boldsymbol{\alpha}(t^n) - \tau\mathbf{H}^{-1}\mathbf{B}(\boldsymbol{\alpha}(t^n)) \tag{29}$$

where τ is the step size. It should be noted that the step size should be small enough to achieve the numerical stability due to the Courant–Friedrichs–Lewy (CFL) condition [31] and to reduce the truncation error due to the variation in a single step of the decent gradient direction and the velocity field in Equation (5) in the level set-based topology optimization methods. After obtaining the approximate solution in Equation (29) at each time step, the time-dependent shape and topology can be updated by using Equation (22).

Therefore, in the present RBF–level set topology optimization method, moving the boundary of the shape along a descent gradient direction is equivalent to transporting the scalar implicit function $\Phi(\mathbf{x})$ by solving the system of coupled non-linear ODEs of Equation (27) and the optimal propagation of the front can be performed by using the approximate solution in Equation (29). It should be noted that the upwind difference methods [30, 36, 37] popular in the conventional level set methods [31, 38] are not employed to advance the front in the present study. Because of the necessary use of upwind differencing at each step, the conventional level set methods have a tendency to lose surface in under-resolved regions [64] or unwanted dissipation of the front [65]. A reinitialization procedure is thus needed to resurrect the behaviour of the level set function $\Phi(\mathbf{x})$ in the neighbourhood of the front to guarantee a good approximation of the normal or the curvature of the front. However, reinitialization error is likely to accumulate as the number of time steps grows. The quite common iterative

reinitialization scheme based on a signed distance function has a potential disadvantage in the relative crudeness of the switch function based on checking the sign of the level set equation, which may cause the front to move [38]. Furthermore, the reinitialization procedure is usually time-consuming [66]. Hence, reinitialization should be avoided as much as possible. In practice, whether reinitialization is appropriate should depend on whether the underlying problem is interested in only the zero level set of function, or the entire function $\Phi(\mathbf{x})$.

In the existing level set-based topology optimization methods in the literature [10, 11], reinitialization produces a severe problem that new holes cannot be created within a material region [39, 40]. In the present RBF–level set method, spatial derivatives of the level set function can be obtained analytically and a good behaviour of the normal or curvature of the front can be maintained due to the infinite smoothness of the MQ splines [45]. Furthermore, reinitialization is not performed and the entire level set function $\Phi(\mathbf{x})$ is taken into account. Thus, the RBF level set model is capable of hole nucleation and elimination of the dependency of the final optimal solution on the design initiation [39]. As suggested by Sethian [38], possible problems with loss of mass or movement of the zero level set without reinitialization can be avoided if an appropriate extension velocity method is adopted. In the present study, a straightforward and efficient extension velocity method is presented, which will be discussed next.

2.5. Extension velocity method

As aforementioned, in the Eulerian approaches the normal velocity $v_n(\mathbf{x})$ at the front must be extended and in the present implementation of the method of lines using collocation the normal velocity $v_n^e(\mathbf{x})$ as shown in Equation (28) is the extension velocity, which is defined over the entire design domain D as $v_n^e(\mathbf{x}) : D \to \mathbb{R}$. The choice of the extension velocity method is crucial since it can directly influence the overall efficiency of the level set method [48]. To guarantee an accurate and efficient time advancement of the front, the extension velocity $v_n^e(\mathbf{x})$ must be defined judiciously.

There are many approaches to constructing the extension velocity $v_n^e(\mathbf{x})$ [38, 66]. The original level set method introduced by Osher and Sethian [30] were concerned with interface problems with geometric propagation velocities and thus a natural construction of an extension velocity can be obtained, in which a signed distance function was used as a level function due to its simplicity. In non-geometric applications, various extension velocity methodologies have also been developed. In many fluid simulations, the fluid velocity was chosen as the extension velocity [67, 68]. An approach using less physical quantity to build an extension velocity field was developed by Sethian and Strain [69], in which a numerical simulation of dendritic solidification with a jump condition across the interface was presented.

When there is no physically meaningful choice available, the extension velocity was suggested to be constructed by extrapolating the velocity from the front by some researchers [70], which requires the location of the closest grid point. Adalsteinsson and Sethian [71] proposed a fast extension method which preserves the signed distance in a narrow band around the zero level set curve by assuming the normal velocity $v_n^e(\mathbf{x})$ be constant along the normal. Ye *et al.* [66] developed a method to deduce the extended velocity from the value of the switching level set function without additional computation by letting the level set function convey information about the image intensity. More recently, Allaire *et al.* [11] extended the normal velocity to the whole domain D by using the 'ersatz material' approach. Due to the intermediate material density, the boundary is always blurry and the extension velocity can thus be regarded as

continuous across the front. Nevertheless, the velocity and the normal may not be smooth at the front and thus another time-consuming PDE procedure was introduced, in addition to the PDE solving reinitialization procedure. Among all these extension velocity methodologies, a signed distance function was often used as the level function and therefore the level function must be reinitialized periodically to preserve the signed distance, which requires a time-consuming PDE solving procedure [38]. Hence, the accuracy and efficiency of the level set methods may be deteriorated [38, 66]. Furthermore, this handling is unnecessary to be physically meaningful.

In the present RBF–level set method, a physically meaningful extension velocity method is proposed for topology optimization based on the implicit level set function. According to Equation (5), a natural extension of the normal velocity can be obtained if the strain field is defined over the entire design domain D by assuming $\boldsymbol{\varepsilon}(\mathbf{u}) = 0,\ \mathbf{u} \in (D \backslash \Omega)$. Since both the strain energy density inside the design domain and the constraint-related Lagrange multiplier are included, this extension velocity is physically meaningful.

Nevertheless, this extension will introduce a discontinuity in the speed close to the front since the strain field is not continuous across the front. To guarantee a smooth progress of the front, this discontinuity should be eliminated. The front itself is smooth and continuously differentiable because of the RBF implicit modelling [53], but the magnitude of the normal velocity at the front may not be continuous and smooth enough due to the finite element modelling involved in the strain analysis. Therefore, the magnitude of the normal velocity along the front should also be smoothed to allow for a stable propagation along a decent gradient direction. To perform all these operations, the front must be explicitly captured.

However, in the field of level set methods, it is well recognized that one of the most notable features of level set methods is that the front need not be explicitly constructed and that all of the method may be executed on the underlying mesh (or grid) [29, 38]. To make full use of this feature, all the smoothing operations are performed in a narrow band region, rather than only along a front curve. A narrow band region around the zero level curve (front) is defined as $\Xi = \{\mathbf{x} \in \mathbb{R}^d \mid |\Phi(\mathbf{x})| \leqslant \delta\}$, where δ is the bandwidth. The extension velocity in the narrow band is further smoothed by using a simple linear filter (radially linear 'hat' kernel [18, 24]) to achieve a good smoothing effect, which can be written as

$$\widehat{v_n^e}(\mathbf{x}) = k^{-1}(\mathbf{x}) \sum_{\mathbf{p} \in N(\mathbf{x})} W_c(\|\mathbf{p} - \mathbf{x}\|) v_n^e(\mathbf{x}) \tag{30}$$

where

$$k(\mathbf{x}) = \sum_{\mathbf{p} \in N(\mathbf{x})} W(\|\mathbf{p} - \mathbf{x}\|) \tag{31}$$

$$W(\|\mathbf{p} - \mathbf{x}\|) = r_{\min} - \|\mathbf{p} - \mathbf{x}\| \tag{32}$$

in which $N(\mathbf{x})$ is the neighbourhood of $\mathbf{x} \in \Xi$ in the filter window and $r_{\min}$ the window size.

Hence, the overall extension velocity is obtained as

$$v_n^e(\mathbf{x}) = \begin{cases} (\boldsymbol{\varepsilon}(\mathbf{u}))^{\mathrm{T}} \mathbf{C} \boldsymbol{\varepsilon}(\mathbf{u}) - \ell & \forall \mathbf{x} \in \mathbb{R}^d \mid \Phi(\mathbf{x}) < -\delta \\ \widehat{v_n^e}(\mathbf{x}) & \forall \mathbf{x} \in \Xi \\ -\ell & \forall \mathbf{x} \in \mathbb{R}^d \mid \Phi(\mathbf{x}) > \delta \end{cases} \tag{33}$$

It can be seen that the present extension velocity field used to move the level set function is closely related with the normal velocity suggested by the physics in the entire design domain and thus the extension velocity conveys information about the physics. Hence, in topology optimization, materials which are not used efficiently such that the strain energy density is too small can be indicated by the extension velocity field with multiple valleys at the undesired locations. As illustrated later, the evolution of the level set function with this extension velocity may finally lead to the creation of a new hole inside the solid domain, similar to the evolutionary structural optimization approach [3], the topological gradient method [39] and the bubble method [72]. This can be a significant improvement over the conventional level set methods, which only allow limited topological changes by splitting or merging connected components [43]. Furthermore, due to the RBF implicit modelling and the linear smoothing effect, the smoothness of the implicit level set function can be well maintained during the time advancement without reinitialization.

3. NUMERICAL EXAMPLES AND DISCUSSION

In this section, numerical examples in two dimensions are presented to illustrate the performance and success of the present RBF–level set method for structural topology optimization. Unless stated otherwise, all the units are consistent and the following parameters are assumed as: the Young's elasticity modulus $E=1$ for solid materials, $E=1\times10^{-5}$ for void materials, and Poisson's ratio $v=0.3$. The implicit function $\Phi(\mathbf{x})$ is initially chosen as a signed distanced function by using the present RBF modelling from a set of given points and no special effort such as reinitialization is made to keep this property during the optimization process.

For all examples, a rectilinear mesh is specified over the design domain for finite element (FE) analysis of the structures. It is also assumed that the knots of the radial basis functions are coincidental to the nodes of the rectilinear mesh. Furthermore, $\delta=1$ for the grid size, $r_{\min}=1.2$ for the narrow band, and $c=10^{-4}$ for the free shape parameter in the RBFs. The present algorithm is terminated when the relative difference between two successive objective function values is less than 10^{-5} or when the given maximum number of iterations has been reached. The FE analysis is based on the bilinear rectangular elements and an 'ersatz material' approach, which is well-known in topology optimization that can be rigorously justified in some cases [11, 17]. In numerical practice of the 'ersatz material' approach, material density is assumed to be piecewise constant in each element and is adequately interpolated in those elements cut by the zero level-set (the shape boundary). The topologies are given in black-and-white form based on the scalar value of the implicit function $\Phi(\mathbf{x})$, as defined in Equation (1). All the CPU time is based on a desktop computer under the MATLAB environment with an Intel Pentium IV processor of 3.40 GHz clock speed.

3.1. Short cantilever beam

The minimum compliance design problem of a short cantilever beam is shown in Figure 4. The whole design domain D is a rectangle of size 2×1 with a fixed boundary ∂D (zero displacement boundary condition) on the left side and a unit vertical point load $P=1$ applied at a fixed non-homogeneous Neumann boundary ∂D_N, the middle point of the right side. The

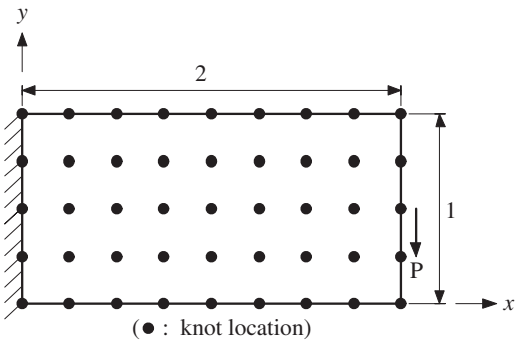

Figure 4. Definition of the minimum compliance design problem of a short cantilever beam.

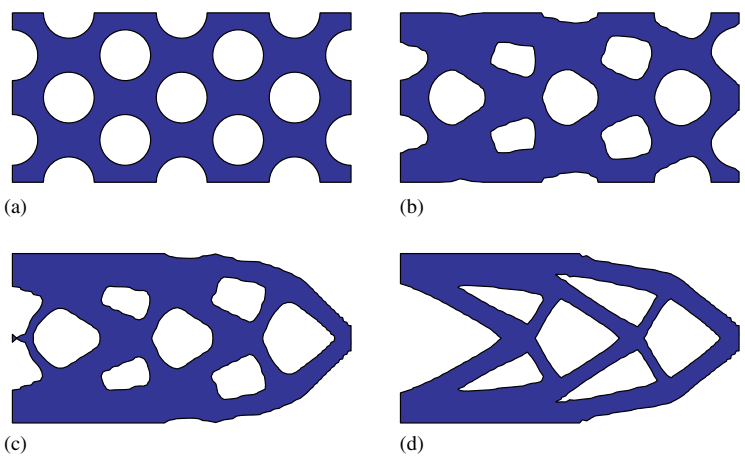

Figure 5. Evolution of an optimal topology: (a) initial design; (b) step 10; (c) step 20; and (d) final design.

objective function is shown in Equation (2) and a fixed Lagrange multiplier $\ell = 20$ is used for the volume constraint.

Figure 5 displays the evolution of an optimal topology of the short cantilever beam with an initial design as shown in Figure 5(a) by using the present RBF–level set method with a 80×40 knot mesh and a time step size $\tau = 10^{-4}$. It can be seen that topological changes and stable evolution have been achieved and the final design as shown in Figure 5(d) is similar to those reported in the literature [11, 40, 47] using the conventional level set methods. Hence, optimal topologies can also be obtained by solving the ODEs in Equation (27), rather than the PDEs in the conventional level set methods [31, 38].

In the present method, the extension normal velocity at each time step is assumed to be constant due to the Euler's method as shown in Equation (29). However, the actual velocity will change with the advancement of the front during each step. Hence, there is a difference Δv_n between the approximate and actual velocities at each point at each time step. Figure 6 shows

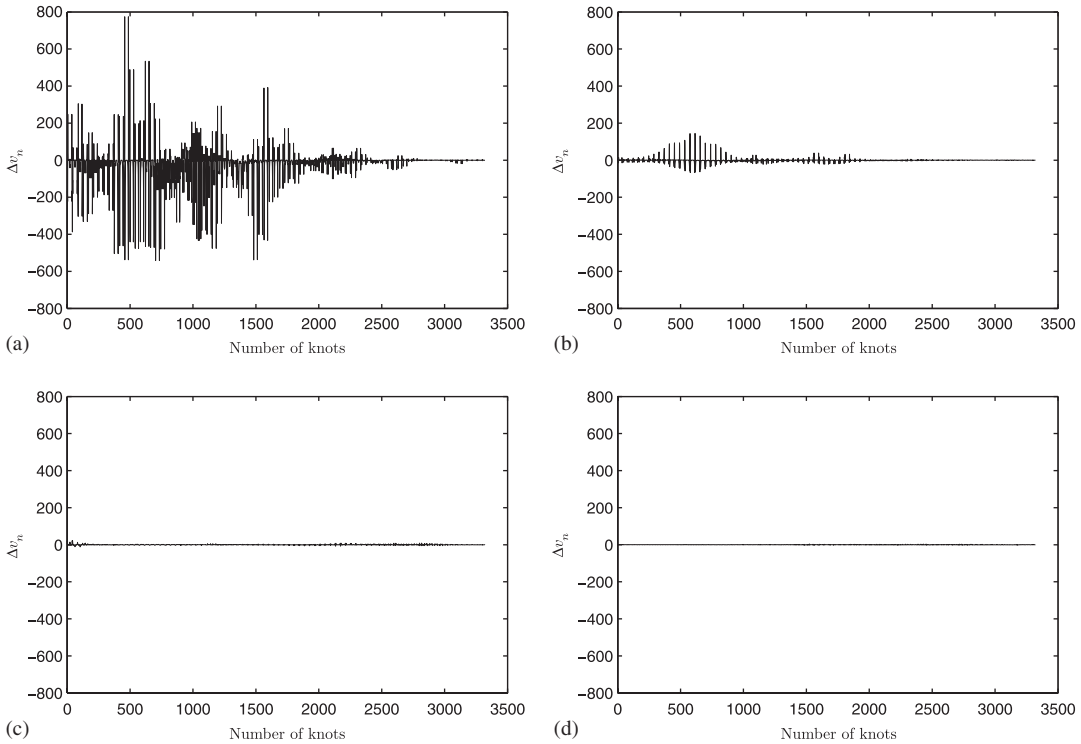

Figure 6. Difference between the approximate and actual velocities Δv_n at each knot: (a) step 1; (b) step 10; (c) step 20; and (d) step 41.

the difference at each knot at the beginning of the specified time steps. It can be seen that the difference will be reduced to minimum with the increase of the time, though a large error can be observed at the first few steps of the evolution. Hence, a stable convergence in the extension velocity field can also be achieved. Furthermore, Figure 7 shows the convergence of the normal velocity at the front, which is defined by only parts of the free boundary of the short cantilever beam in this study. It can be seen that there is a big difference between the approximate and actual velocities in both magnitude and direction in the first few steps, however, this difference will be globally eliminated with the evolution. Both the approximate and actual velocities at the front will converge to zero, which agrees well with the theoretical prediction that the necessary condition of topology optimization based on shape sensitivity is that the normal velocity is zero on the boundary [11], as shown in Equation (4). Figure 8 displays the scalar extension velocity field ($v_n^e \geqslant 0$) for this short cantilever beam. Comparing Figure 8 with Figures 5(d) and 7(f), it can be seen that the normal velocity can be approximated as zero on the boundary of the final design. The extension normal velocity, as defined in Equation (33), is relatively high at the stress concentration regions around the fixed boundary and the loading point because of the high strain energy density.

Figure 9 displays the effect of the mesh discretization and time step size on the convergence speed of the objective function for the short cantilever beam. Final topologies similar to the one

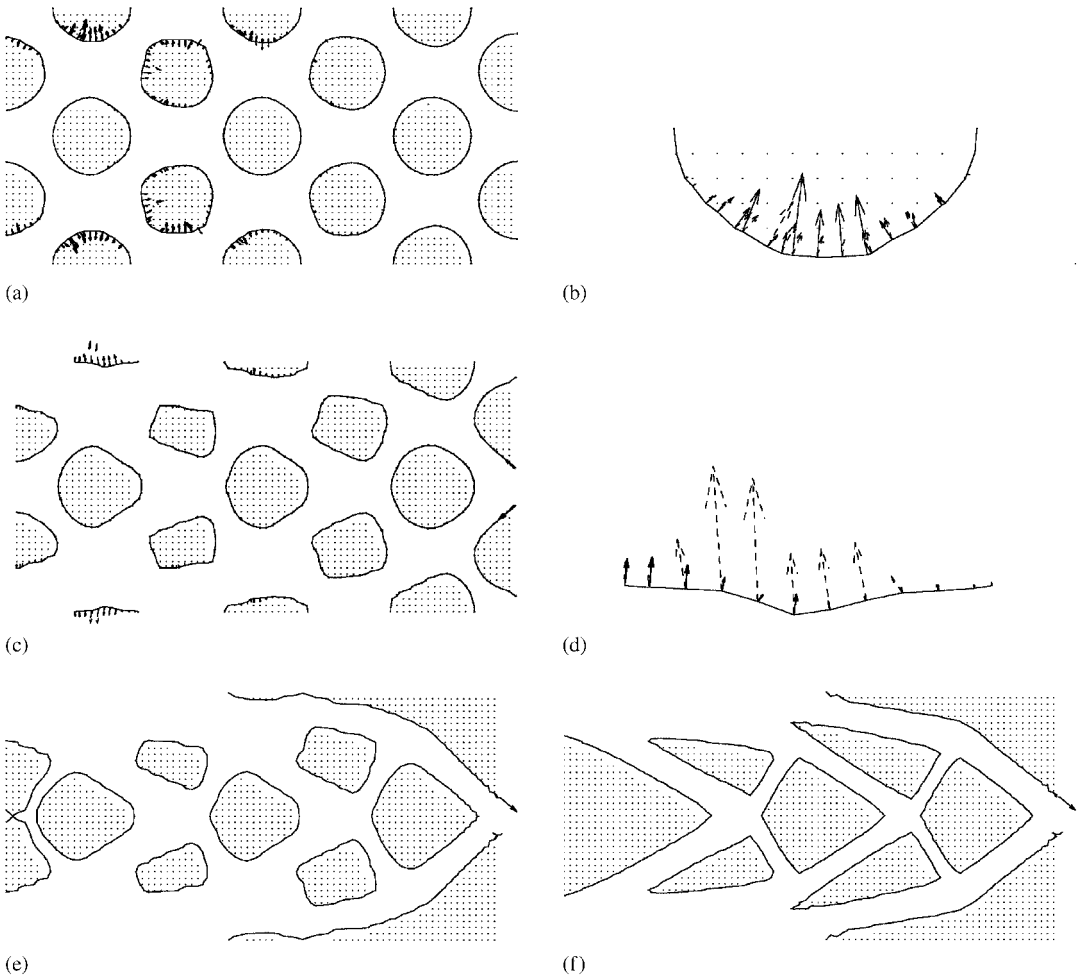

Figure 7. Convergence of the normal velocity at the front (solid arrow: actual velocity; dashed arrow: approximate velocity; solid curve: front position): (a) step 1; (b) local Δv_n at step 1; (c) step 10; (d) local Δv_n at step 10; (e) step 20; and (f) step 41.

shown in Figure 5(d) can be obtained by using a smaller step size $\tau = 10^{-4}$ for all the three mesh discretizations or a larger step size $\tau = 10^{-3}$ for finer mesh discretizations 60×30 and 80×40 only, while a different final topology (sub-optimum) shown in Figure 10 is produced if a larger time step $\tau = 10^{-3}$ is used for the coarse mesh discretization 40×20. It appears that the final design is more sensitive to the time step size. As aforementioned, the step size should be small enough to satisfy the CFL condition [31] and to reduce the truncation error. In practical terms, this means that the time step size will be related to the grid resolution [35] and therefore a smaller step size should be used for a coarser mesh. A larger step size used in the coarse mesh 40×20 would not result in the movement of the front along the descent direction, as shown in Figure 9(a), due to the larger errors in the estimation of the normal velocity field,

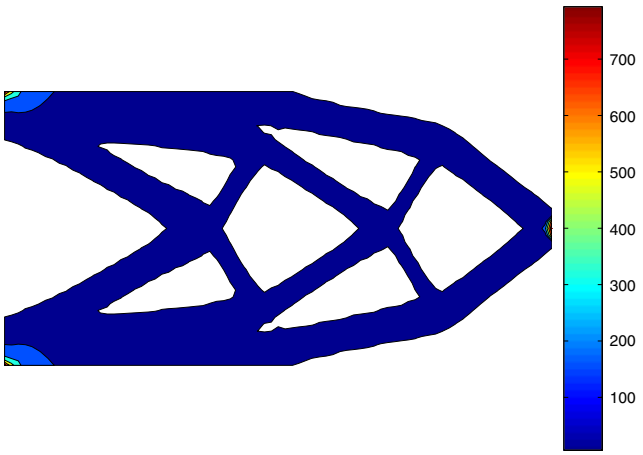

Figure 8. Scalar normal velocity field ($v_n \gtrless 0$) for the short cantilever beam.

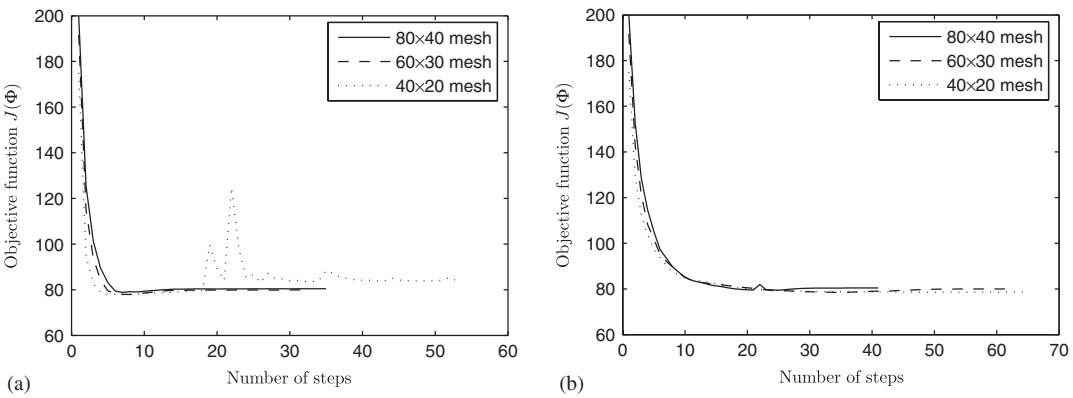

Figure 9. Convergence speed of the objective function for the short cantilever beam: (a) $\tau = 10^{-3}$; and (b) $\tau = 10^{-4}$.

as discussed in detail in Reference [47]. The final solution may converge to a local optimum, as shown in Figure 10, due to the local search nature of the present optimization method. It should be noted that the structural topology optimization problems have many solutions such as one global and many local minima [18, 73].

The effect of the free shape parameter c of the MQ splines shown in Equation (8) in the present RBF modelling of the implicit function $\Phi(\mathbf{x})$ on the convergence speed of the objective function $J(\Phi)$ is studied next. As shown in Table II, the free parameter c may affect the convergence speed significantly. For the relatively coarse mesh 40×20, to increase the magnitude of the shape parameter c in the range $c \in [0.0001, 0.1]$ can make the convergence speed faster, though the objective function value may become a bit worse. This is consistent with the theoretical results in Reference [56] that the flatter the basis function used for interpolation,

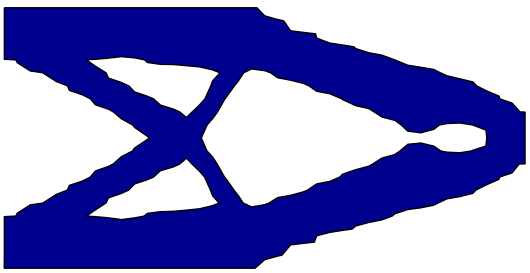

Figure 10. Final topology for the short cantilever beam using a 40×20 mesh and a time step $\tau = 10^{-3}$.

Table II. RBF modelling with different shape parameters for the short cantilever beam ($\tau = 10^{-4}$). (T_0: total CPU time; N_{it}: total number of iterations).

c	Mesh size	$J(\Phi)$	$T_0(s)$	N_{it}	Remark
0.0001	80×40	80.403	1.402e + 004	41	—
	60×30	79.972	7.111e + 003	63	—
	40×20	78.600	1.705e + 003	65	—
0.001	80×40	80.299	9.761e + 003	34	—
	60×30	79.997	4.595e + 003	59	—
	40×20	78.727	5.438e + 002	34	—
0.01	80×40	78.561	1.046e + 004	39	—
	60×30	80.252	4.916e + 003	62	—
	40×20	78.709	5.234e + 002	33	—
0.1	80×40	—	—	—	No convergence
	60×30	89.349	7.965e + 003	100	—
	40×20	79.071	4.442e + 002	28	—

the more accurate the approximation. However, Table II also shows that for the fine meshes 80×40 and 60×30, the corresponding convergence speed can be deteriorated by a larger shape parameter ($c \in [0.01, 0.1]$). The reason can be that, according to Schaback's uncertainty principle [74], there is a trade-off between the accuracy gained in interpolation by increasing the parameter c and the stability lost due to the large matrix condition number created [56]. Hence, if the mesh size h is reduced for better accuracy, the shape parameter c must also be reduced correspondingly to maintain matrix stability since the matrix condition number is dependent on the parameter c/h [56].

For this example, effect of the initial designs with fewer holes than the final design as shown in Figure 5(d) is also investigated. The initial design with a single internal hole as shown in Figure 11(a) is first studied. The evolution of the corresponding optimal topology is displayed in Figure 11, in which a 80×40 mesh and a time step size $\tau = 10^{-4}$ are used and a volume fraction of $f = 0.50$ is applied as a volume constraint to avoid getting stuck at a local optimum

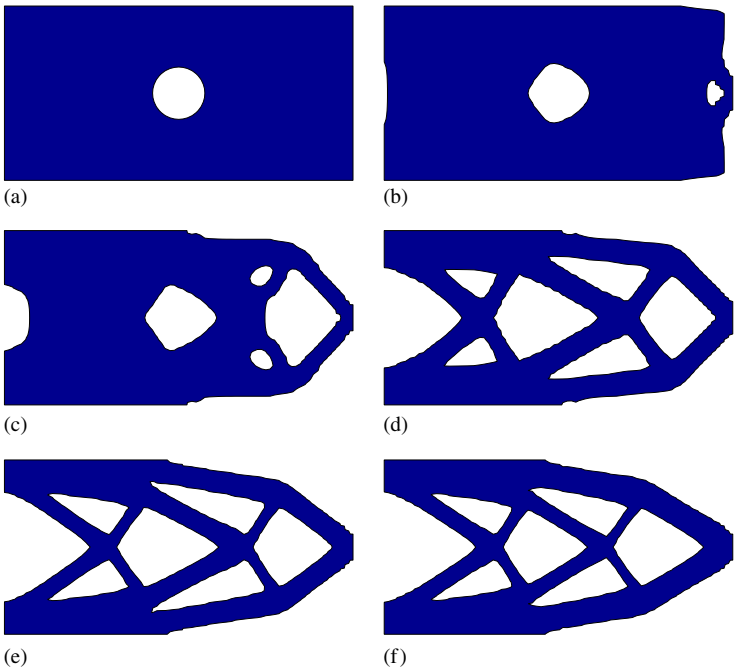

Figure 11. Evolution of an optimal topology with an initial design with one central hole only: (a) initial design; (b) step 16; (c) step 22; (d) step 28; (e) step 60; and (f) final design.

with a small hole. It can be seen that topological changes to create new holes can be achieved and the final design shown in Figure 11(f) is similar to the one shown in Figure 5(d).

In the conventional level set methods, the nucleation of new holes is not allowed and thus a bubble or topological gradient method has to be introduced and incorporated into the level set methods, as shown in References [39, 40]. Since both the topological and shape derivatives are used in a modified level set method, it would be quite difficult to switch between them in an automatic way [39, 40]. Furthermore, it is also very difficult for the topological derivative to handle surface functions [43]. In the present RBF–level set method, the topological derivative is not used and the creation of new holes can be fulfilled by using the shape derivative only, together with the present extension velocity without reinitialization. Figure 12 shows the variation of the implicit function $\Phi(\mathbf{x})$ with the advancement of the front. Although in the initial design $\Phi(\mathbf{x})$ is built as a signed distance function, as shown in Figure 12(a), this property is not preserved during the present evolution of the optimal topology without reinitialization and thus the distribution of $\Phi(\mathbf{x})$ may have many valleys with high gradients for an admissible design after some iterations. As shown in Figure 12(a), there is a valley with a high gradient $\nabla\boldsymbol{\Phi}$ near the loading point at iteration 16 and correspondingly an internal hole near this valley has been created due to this high gradient. This kind of nucleation of new holes can be justified by the variation of the objective function $J(\Phi)$. Figure 13 displays the convergence speed of the objective function and the volume constraint. It can be seen that with the creation of new holes the present method can successfully move out of the infeasible region with a high volume

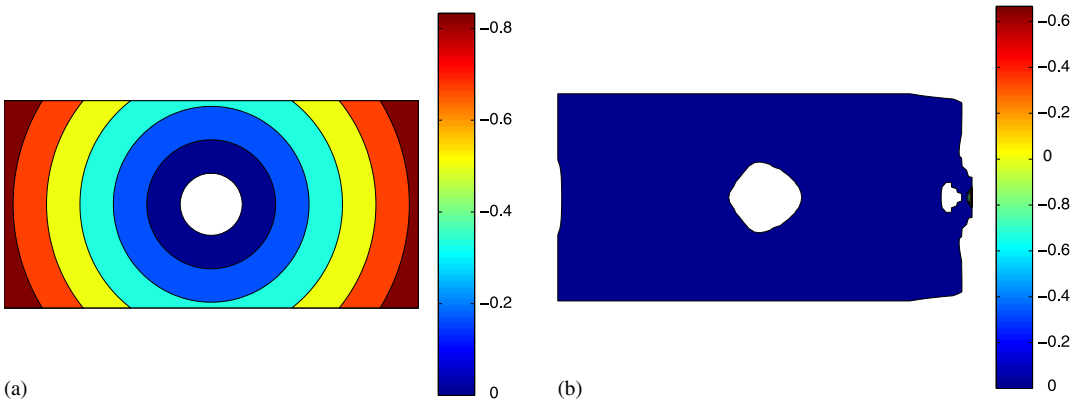

Figure 12. Variation of the implicit function $\Phi(\mathbf{x}) \leqslant 0$ for the short cantilever beam: (a) initial design; and (b) step 16.

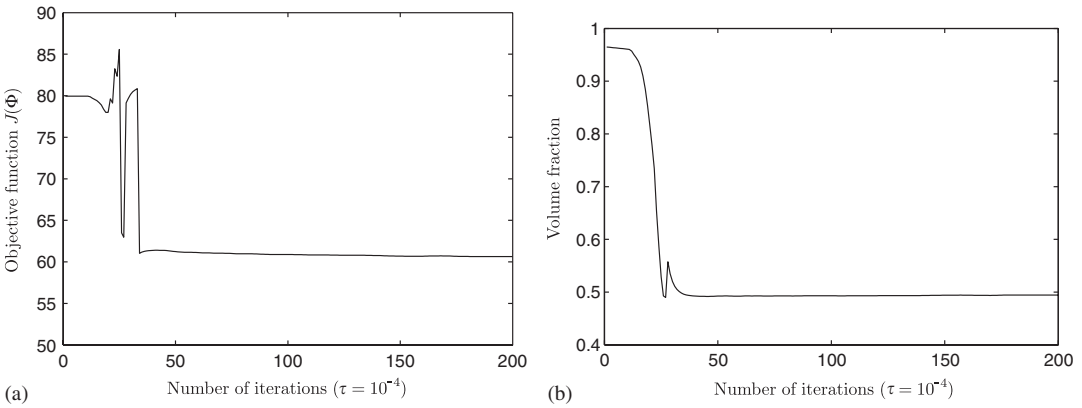

Figure 13. Convergence speed of the objective function and the volume constraint for the short cantilever beam: (a) objective function; and (b) volume fraction.

fraction of $f = 0.965$ and enter a feasible region with a lower volume fraction ($f \leqslant 0.50$), as shown in Figure 13(b). The bumps in the convergence curve shown in Figure 13(a) is due to a significant change of topology. Since the initial designs shown in Figures 5(a) and 11(a) are totally different while the final designs shown in Figures 5(d) and 11(f) are almost the same, it can be concluded that the present RBF–level set method can largely eliminate the dependency on the initial design. It should be noted that in the conventional level set methods [11, 40] the final design is highly dependent on the initial design.

To further demonstrate that the initial designs with fewer holes than the final design as shown in Figure 5(d) do not affect the final designs significantly, initial designs without any internal holes are also considered. Figure 14 displays the evolution history of an optimal topology with a symmetric initial design without a hole as shown in Figure 14(a). Again, it can be

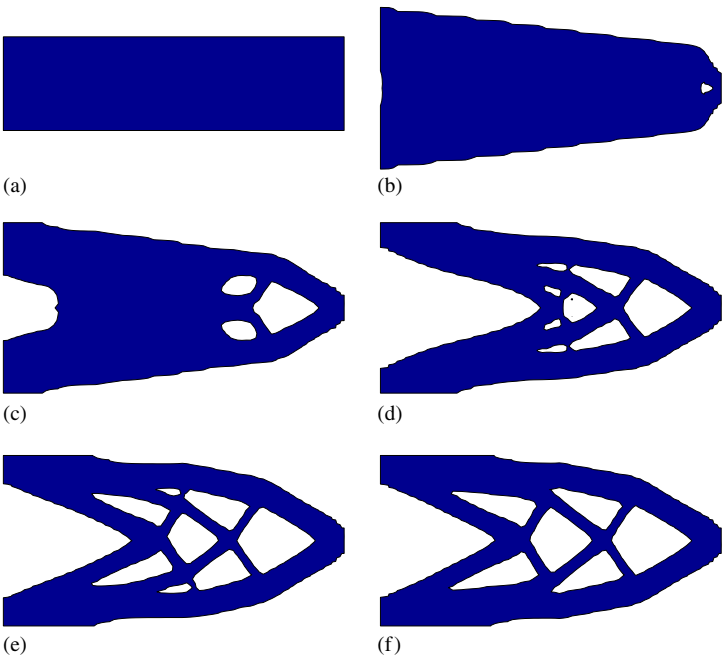

Figure 14. Evolution of an optimal topology with a symmetric initialization without a hole: (a) symmetric initial design; (b) step 15; (c) step 24; (d) step 50; (e) step 100; and (f) final design.

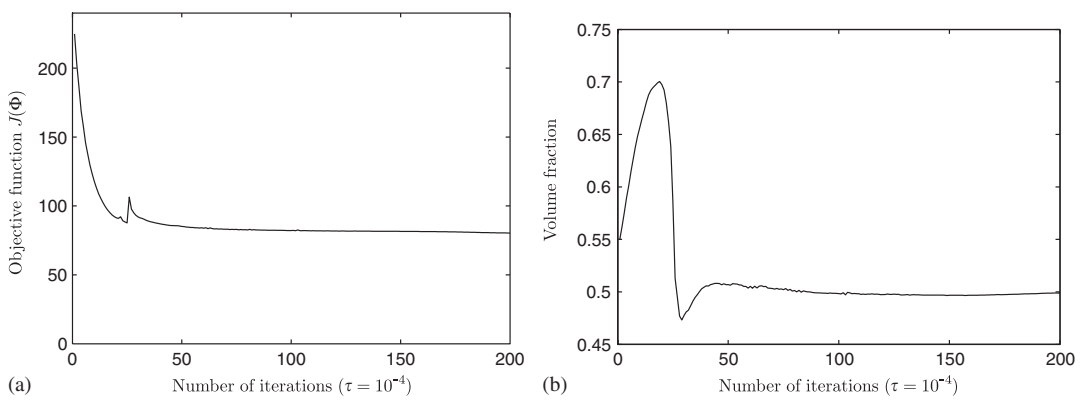

Figure 15. Convergence speed of the objective function and the volume constraint for the short cantilever beam with a symmetric initial design without a hole: (a) objective function; and (b) volume fraction.

seen that topological changes to create new holes can be well achieved and the final design shown in Figure 14(f) is almost identical to the one shown in Figure 5(d). Figure 15 shows the convergence speed of the objective function and the volume constraint. Since the objective

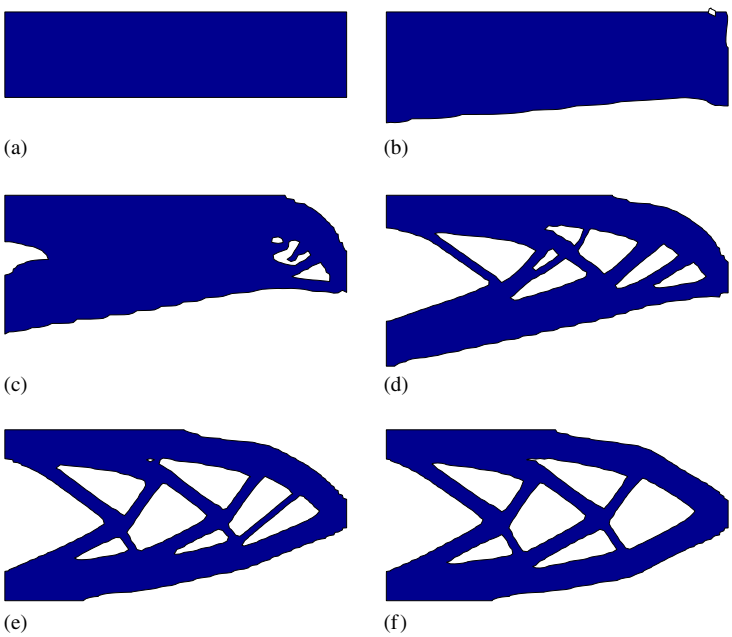

Figure 16. Evolution of an optimal topology with an unsymmetrical initialization without a hole: (a) unsymmetrical initial design; (b) step 8; (c) step 16; (d) step 32; (e) step 60; and (f) final design.

function $J(\Phi)$ decreases significantly with the time advancement, the nucleation of new holes as shown in Figure 14 can be justified. Figure 16 displays the evolution history of an optimal topology with an unsymmetrical initial design without a hole shown in Figure 16(a), in which the top half of the rectangular design domain is solid and the other half empty. It can be seen that topological changes due to the nucleation of new holes have also been achieved and the final design shown in Figure 16(f) is nearly the same as the one shown in Figure 5(d). Hence, the present method is less sensitive to initialization than the conventional level set methods [11, 40]. Furthermore, Figure 17 shows the convergence speed of the objective function and the volume constraint. It can be found that the objective function $J(\Phi)$ decreases drastically from about 290 to quite below 100 after 30 iterations and the present method will smoothly converge to a (local) minimum even if the initial design is unsymmetrical and without holes.

3.2. MBB beam

The minimum compliance design problem of a Messerschmitt–Bölkow–Blohm (MBB) beam is also investigated in the present study. The MBB beam, as shown in Figure 18, is loaded with a concentrated vertical force of P at the centre of the top edge and is supported on rollers at the bottom-right corner and on fixed supports at the bottom-left corner. The basic parameters are assumed to be $L=4$, $H=1$, thickness $t=1.0$, load $P=1$ and the fixed Lagrange multiplier $\ell=10$. It is also assumed that the time step size $\tau=10^{-3}$ and the mesh size 120×30. The initial design of this problem is shown in Figure 19, in which circular holes are used for

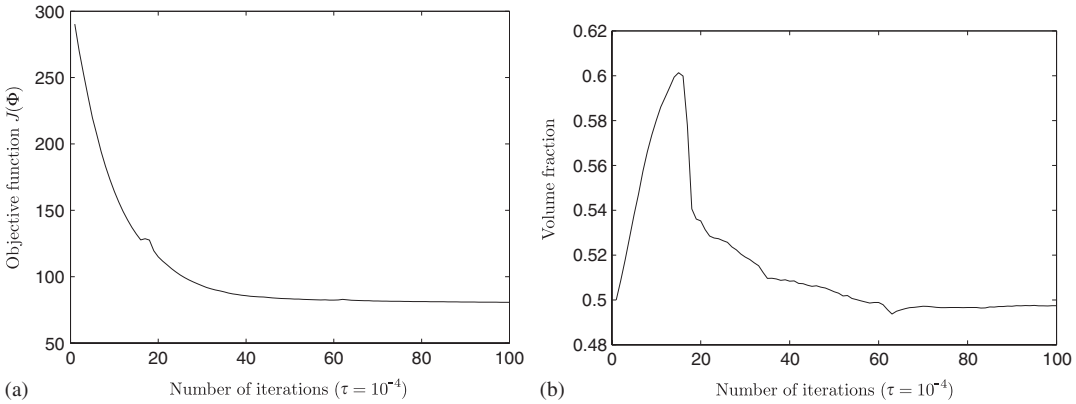

Figure 17. Convergence speed of the objective function and the volume constraint for the short cantilever beam with an unsymmetrical initial design without a hole: (a) objective function; and (b) volume fraction.

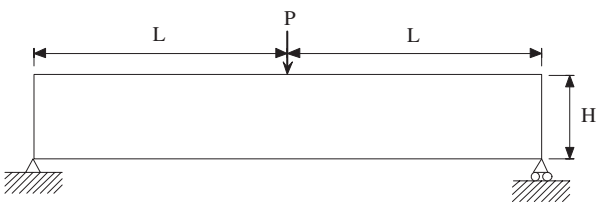

Figure 18. Definition of the minimum compliance design problem of a MBB beam.

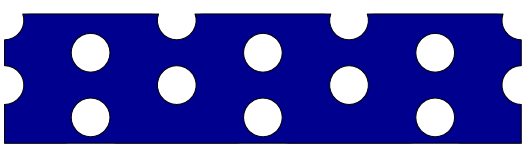

Figure 19. Initial design for the minimum compliance design problem of a MBB beam.

the initialization. Figure 20 shows the extension velocities at each knot and the front for the initial and final designs. It can be seen that extension velocities at the front converges to zero as theoretically predicted. The extension velocity inside the solid domain may not necessarily be zero and the maximum value lies in the stress concentration regions. Figure 21 shows the final design of this MBB beam problem. It can be seen that the final design is similar to a truss structure with hinge-like or pin connection at the bottom joints since the external force is applied at the top joint only and thus the resultant moment for each bar member would be small enough.

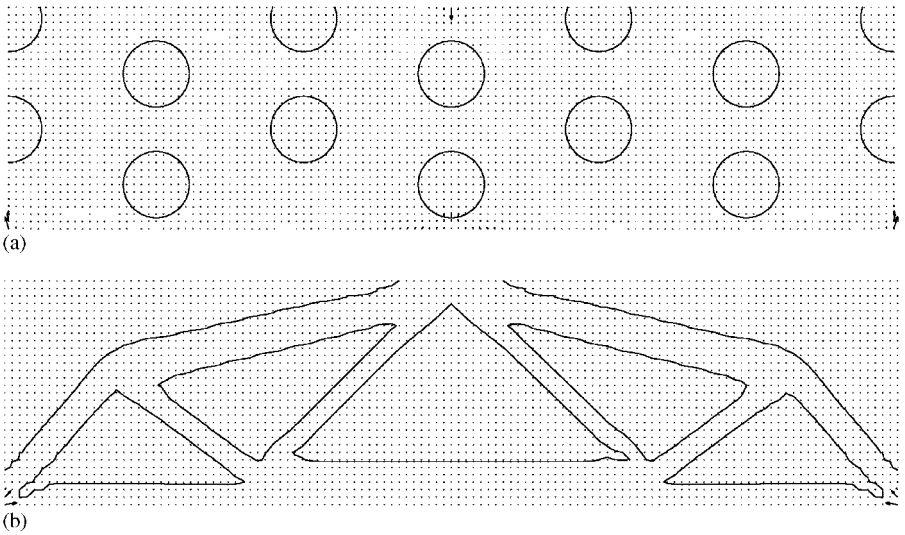

Figure 20. Front and extension velocity for the MBB beam: (a) initial front and extension velocity; and (b) final front and extension velocity.

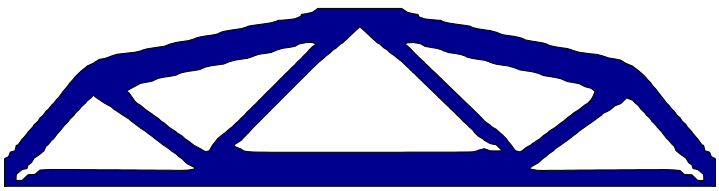

Figure 21. Final design for the minimum compliance design problem of a MBB beam.

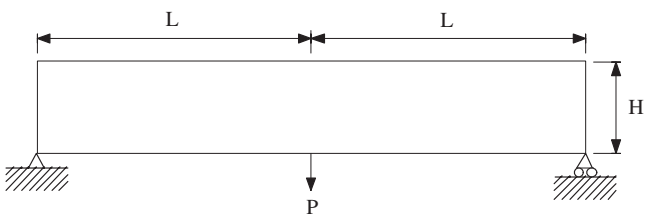

Figure 22. Definition of the minimum compliance design problem of a Michell type structure.

3.3. Michell type structure

The minimum compliance design problem of a Michell type structure [75] is used to further illustrate the performance of the present RBF–level set method. The Michell type structure, as shown in Figure 22, is loaded with a concentrated vertical force of P at the centre of the

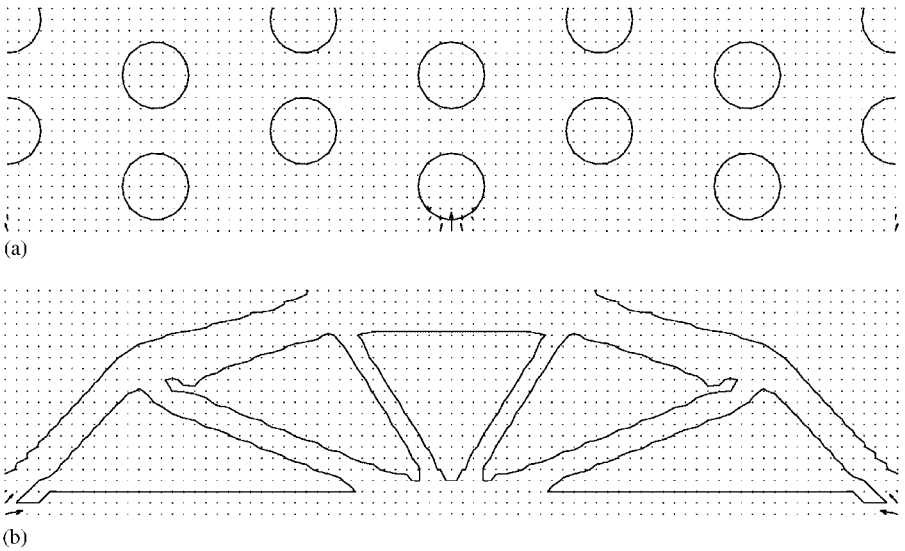

Figure 23. Front and extension velocity for the Michell type structure: (a) initial front and extension velocity; and (b) final front and extension velocity.

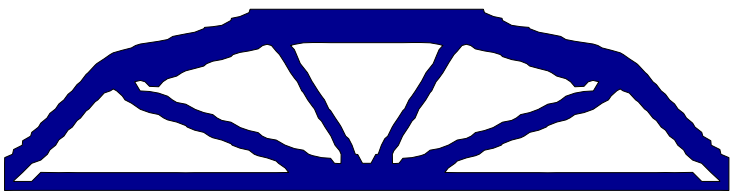

Figure 24. Final design for the minimum compliance design problem of a Michell type structure.

bottom edge and is supported on rollers at the bottom-right corner and on fixed supports at the bottom-left corner. The basic parameters are assumed to be $L=4$, $H=1$, thickness $t=1.0$, load $P=1$ and the fixed Lagrange multiplier $\ell=10$. It is also assumed that the time step size $\tau=10^{-4}$ and the mesh size 80×20. Since the definition of the design domain is quite similar to that of the MBB beam shown in Figure 18 except the position of the loading point, the initial design shown in Figure 19 is also adopted as the initial design for this Michell type structure. Figure 23 shows extension velocities at each knot and the front for the initial and final designs. Again, the extension velocities at the front converges to zero as theoretically predicted. The extension velocity inside the solid domain is not all zero and the maximum value lies in the stress concentration regions. Figure 24 displays the final design of this problem. Again, this final design is quite similar to a truss structure with pin-like connection at some joints since the external force is applied at a bottom joint only and thus the resultant moment for each bar member is small. Comparing Figure 24 with Figure 21, it can be seen that a change of the loading point can result in drastic changes in the final design, similar to the observation in Reference [18].

4. CONCLUSIONS

In this study, a RBF–level set method is proposed for structural topology optimization. Radial basis functions popular in scattered data fitting and function approximation are incorporated into the conventional level set methods to construct a more efficient level set method for topology optimization. The implicit level set function is approximated by using the RBF implicit model with MQ splines and a high level of accuracy and smoothness even in the gradient and curvature of the implicit function is thus achieved. By assuming that the time dependence of the implicit function is due to the generalized expansion coefficients of the RBF interpolant, the Hamilton–Jacobi PDE is converted into a mathematically more convenient ODE and the original time dependent initial value problem is changed to a relatively simple interpolation problem for the initial values of the generalized expansion coefficients. A collocation formulation of the method of lines is developed and a system of non-linear coupled ODEs are obtained.

Furthermore, a physically meaningful and efficient extension velocity method is presented to eliminate the discontinuities and to allow smooth propagation at the front of the implicit function. Potential problems without reinitialization in the conventional level set method can be alleviated. This proposed RBF–level set method is implemented in the framework of topological optimum of minimum compliance design and its higher efficiency and accuracy over the conventional level set methods are illustrated. Numerical examples of 2D structures are chosen to show the success of the present method in accuracy, convergence speed and insensitivity to initial designs. Compared with the conventional level set method, the present method can generate similar optimal designs without the numerically more complicated PDE solving procedures and, furthermore, it can largely eliminate the dependency on initial designs due to its ability in the nucleation of new holes. It is suggested that the introduction of the radial basis functions to the conventional level set methods possesses promising potentials in structural topology optimization.

ACKNOWLEDGEMENTS

This research work is supported in parts by the Research Grants Council of Hong Kong SAR (Project No. CUHK4164/03E), a Post-doctoral Fellowship from the Chinese University of Hong Kong (No. 04/ENG/1), and the Natural Science Foundation of China (NSFC) (Grants No. 50128503 and No. 50390063), which the authors gratefully acknowledge.

REFERENCES

1. Rozvany GIN. Aims, scope, methods, history and unified terminology of computer-aided topology optimization in structural mechanics. *Structural and Multidisciplinary Optimization* 2001; **21**(2):90–108.
2. Bendsøe MP, Kikuchi N. Generating optimal topologies in structural design using a homogenization method. *Computer Methods in Applied Mechanics and Engineering* 1988; **71**:197–224.
3. Xie YM, Steven GP. A simple evolutionary procedure for structural optimization. *Computers and Structures* 1993; **49**(5):885–896.
4. Bendsøe MP, Sigmund O. Material interpolations in topology optimization. *Archive of Applied Mechanics* 1999; **69**:635–654.
5. Tai K, Chee TH. Design of structures and compliant mechanisms by evolutionary optimization of morphological representations of topology. *ASME Journal of Mechanical Design* 2000; **122**(4):560–566.
6. Sigmund O. Design of multiphysics actuators using topology optimization. Part 1: one material structures. *Computer Methods in Applied Mechanics and Engineering* 2001; **190**(49–50):6577–6604.

7. Tai K, Cui GY, Ray T. Design synthesis of path generating compliant mechanisms by evolutionary optimization of topology and shape. *ASME Journal of Mechanical Design* 2002; **124**(3):492–500.
8. Belytschko T, Xiao SP, Parimi C. Topology optimization with implicit functions and regularization. *International Journal for Numerical Methods in Engineering* 2003; **57**(8):1177–1196.
9. Hamda H, Jouve F, Lutton E, Schoenauer M, Sebag M. Compact unstructured representations for evolutionary design. *Applied Intelligence* 2002; **16**(2):139–155.
10. Wang MY, Wang X, Guo D. A level set method for structural topology optimization. *Computer Methods in Applied Mechanics and Engineering* 2003; **192**:227–246.
11. Allaire G, Jouve F, Toader AM. Structural optimization using sensitivity analysis and a level-set method. *Journal of Computational Physics* 2004; **194**:363–393.
12. Guest JK, Prevost JH, Belytschko T. Achieving minimum length scale in topology optimization using nodal design variables and projection functions. *International Journal for Numerical Methods in Engineering* 2004; **61**(2):238–254.
13. Wang SY, Tai K. Graph representation for evolutionary structural topology optimization. *Computers and Structures* 2004; **82**(20–21):1609–1622.
14. Wang SY, Tai K. Structural topology design optimization using genetic algorithms with a bit-array representation. *Computer Methods in Applied Mechanics and Engineering* 2005; **194**(36–38):3749–3770.
15. Wang SY, Tai K. Bar-system representation method for structural topology optimization using the genetic algorithms. *Engineering Computations* 2005; **22**(2):206–231.
16. Wang MY, Wang SY. Bilateral filtering for structural topology optimization. *International Journal for Numerical Methods in Engineering* 2005; **63**(13):1911–1938.
17. Allaire G. *Shape Optimization by the Homogenization Method*. Springer: New York, 2001.
18. Bendsøe MP, Sigmund O. *Topology Optimization*: *Theory*, *Methods and Applications*. Springer: Berlin, 2003.
19. Bendsøe MP. Optimal shape design as a material distribution problem. *Structural Optimization* 1989; **1**:193–202.
20. Bendsøe MP, Diaz AR, Kikuchi N. Topology and generalized layout optimization of elastic structures. In *Topology Design of Structures*, Bendsøe MP, Soares CAM (eds), NATO ASI Series E, vol. 227. Kluwer Academic Publishers: Dordrecht, 1993; 159–206.
21. Yin L, Ananthasuresh GK. Topology optimization of compliant mechanisms with multiple materials using a peak function material interpolation scheme. *Structural and Multidisciplinary Optimization* 2001; **23**(1):49–62.
22. Hassani B, Hinton E. *Homogenization and Structural Topology Optimization*: *Theory*, *Practice and Software*. Springer: London, 1999.
23. Bulman S, Sienz J, Hinton E. Comparisons between algorithms for structural topology optimization using a series of benchmark studies. *Computers and Structures* 2001; **79**(12):1203–1218.
24. Sigmund O. A 99 line topology optimization code written in MATLAB. *Structural and Multidisciplinary Optimization* 2001; **21**(2):120–127.
25. Rozvany GIN, Zhou M, Birker T. Generalized shape optimization without homogenization. *Structural Optimization* 1992; **4**:250–254.
26. Xie YM, Steven GP. *Evolutionary Structural Optimization*. Springer: U.K., 1997.
27. Rozvany GIN. Stress ratio and compliance based methods in topology optimization—A critical review. *Structural and Multidisciplinary Optimization* 2001; **21**:109–119.
28. Sethian JA, Wiegmann A. Structural boundary design via level set and immersed interface methods. *Journal of Computational Physics* 2000; **163**(2):489–528.
29. Wang MY, Wang X. PDE-driven level sets, shape sensitivity and curvature flow for structural topology optimization. *Computer Modeling in Engineering and Sciences* 2004; **6**(4):373–395.
30. Osher S, Sethian JA. Front propagating with curvature dependent speed: algorithms based on Hamilton–Jacobi formulations. *Journal of Computational Physics* 1988; **78**:12–49.
31. Osher SJ, Fedkiw RP. *Level Set Methods and Dynamic Implicit Surfaces*. Springer: New York, 2002.
32. Osher S, Santosa F. Level-set methods for optimization problems involving geometry and constraints: frequencies of a two-density inhomogeneous drum. *Journal of Computational Physics* 2001; **171**:272–288.
33. Tornberg AK, Engquist B. Numerical approximations of singular source terms in differential equations. *Journal of Computational Physics* 2004; **200**:462–488.
34. Wang MY, Wang X. A level-set based variational method for design and optimization of heterogeneous objects. *Computer-Aided Design* 2005; **37**:321–337.
35. Mitchell IM. A toolbox of level set methods. *Technical Report TR-2004-09*, Department of Computer Science, University of British Columbia, Canada, 2004.

36. Osher S, Shu CW. High-order essentially nonoscillatory schemes for Hamilton–Jacobi equations. *SIAM Journal on Numerical Analysis* 1991; **28**:907–922.
37. Jiang GS, Peng D. Weighted ENO schemes for Hamilton–Jacobi equations. *SIAM Journal on Scientific Computing* 2000; **21**:2126–2143.
38. Sethian JA. *Level Set Methods and Fast Marching Methods*. Cambridge Monographs on Applied and Computational Mathematics (2nd edn). Cambridge University Press: Cambridge, U.K., 1999.
39. Burger M, Hackl B, Ring W. Incorporating topological derivatives into level set methods. *Journal of Computational Physics* 2004; **194**:344–362.
40. Allaire G, Gournay FD, Jouve F, Toader AM. Structural optimization using topological and shape sensitivity via a level set method. *Internal Report 555*, Ecole Polytechnique, France, 2004.
41. Wang X, Mei Y, Wang MY. Incorporating topology/phase derivatives into level set methods for optimization of solids. *WISDOM 2004-Warsaw International Seminar on Design and Optimal Modeling*. Warsaw, Poland, 2004.
42. Wang MY, Wei P. Topology optimization with level set method incorporating topological derivative. *6th World Congress on Structural and Multidisciplinary Optimization*. Rio de Janeiro, Brazil, 2005.
43. Burger M. Lecture notes on infinite-dimensional optimization and optimal design. *Report 285J*, University of California, Los Angeles, CA, U.S.A., 2004.
44. Buhmann MD. *Radial Basis Functions*: *Theory and Implementations*. Cambridge Monographs on Applied and Computational Mathematics, vol. 12. Cambridge University Press: New York, NY, 2004.
45. Kansaa EJ, Powerb H, Fasshauerc GE, Ling L. A volumetric integral radial basis function method for time-dependent partial differential equations. I. Formulation. *Engineering Analysis with Boundary Elements* 2004; **28**:1191–1206.
46. Borrvall T, Petersson J. Topology optimization using regularized intermediate mass density. *Computer Methods in Applied Mechanics and Engineering* 2001; **190**:4911–4928.
47. Wang SY, Wang MY. A moving superimposed finite element method for structural topology optimization. *International Journal for Numerical Methods in Engineering* 2005, in press.
48. Richards DF, Bloomfield MO, Sen S, Calea TS. Extension velocities for level set based surface profile evolution. *Journal of Vacuum Science and Technology A* 2001; **19**(4):1630–1635.
49. Osher S, Fedkiw RP. Level set methods: an overview and some recent results. *Journal of Computational Physics* 2001; **169**:463–502.
50. Peng D, Merriman B, Osher S, Zhao H, Kang M. A PDE-based fast local level set method. *Journal of Computational Physics* 1999; **155**:410–438.
51. Kim NH, Chang Y. Eulerian shape design sensitivity analysis and optimization with a fixed grid. *Computer Methods in Applied Mechanics and Engineering* 2005; **194**(30–33):3291–3314.
52. Cecil T, Qian JL, Osher S. Numerical methods for high dimensional Hamilton–Jacobi equations using radial basis functions. *Journal of Computational Physics* 2004; **196**(1):327–347.
53. Kansa EJ. Multiquadrics—A scattered data approximation scheme with applications to computational fluid dynamics: I. Surface approximations and partial derivative estimates. *Computers and Mathematics with Applications* 1990; **19**:127–145.
54. Carr JC, Beatson RK, Cherrie JB, Mitchell TJ, Fright WR, McCallum BC, Evans TR. Reconstruction and representation of 3D objects with radial basis functions. *ACM SIGGRAPH 2001*, Los Angeles, CA, 2001; 67–76.
55. Morse BS, Yoo TS, Chen DT, Rheingans P, Subramanian KR. Interpolating implicit surfaces from scattered surface data using compactly supported radial basis functions. *SMI '01*: *Proceedings of the International Conference on Shape Modeling and Applications*. IEEE Computer Society: Washington, DC, U.S.A., 2001; 89–98.
56. Cheng AD, Golberg MA, Kansa EJ, Zammito G. Exponential convergence and H-c multiquadric collocation method for partial differential equations. *Numerical Methods for Partial Equations* 2003; **19**(5):571–594.
57. Hardy RL. Theory and applications of the multiquadric-biharmonic method: 20 years of discovery. *Computers and Mathematics with Applications* 1990; **19**(8/9):163–208.
58. Micchelli CA. Interpolation of scattered data: distance matrices and conditionally positive definite. *Constructive Approximation* 1986; **2**:11–22.
59. Madych WR, Nelson SA. Bounds on multivariate polynomials and exponential error estimates for multiquadric interpolation. *Journal of Approximation Theory* 1992; **70**:94–114.
60. Franke R. Scattered data interpolation: tests of some methods. *Mathematics of Computation* 1982; **38**:181–200.
61. Greengard L, Rokhlin V. A fast algorithm for particle simulations. *Journal of Computational Physics* 1987; **73**:325–348.

62. Madsen NK. The method of lines for the numerical solution of partial differential equations. *ACM SIGNUM Newsletter* 1975; **10**(4):5–7.
63. Greenberg MD. *Advanced Engineering Mathematics* (2nd edn). Prentice-Hall: Upper Saddle River, New Jersey, U.S.A., 1998.
64. Lageneste LDD, Pitsch H. A numerical scheme for the large-eddy simulation of turbulent combustion using a level-set method. *Annual Research Briefs*, *Center for Turbulence Research*, Stanford University, Standford, CA, U.S.A., 2002.
65. Sussman M, Fatemi E. An efficient, interface-preserving level set re-distancing algorithm and its application to interfacial incompressible fluid flow. *SIAM Journal on Scientific Computing* 1999; **20**:1165–1191.
66. Ye JC, Bresler Y, Moulin P. A self-referencing level-set method for image reconstruction from sparse Fourier samples. *International Journal of Computer Vision* 2002; **50**(3):253–270.
67. Sussman M, Smereka P, Osher S. A level-set approach for computing solutions to incompressible two-phase flow. *Journal of Computational Physics* 1994; **114**:146–159.
68. Rhee CW, Talbot L, Sethian JA. Dynamical behavior of a premixed open V-flame. *Journal of Fluid Mechanics* 1995; **300**:87–115.
69. Sethian JA, Strain JD. Crystal growth and dendritic solidification. *Journal of Computational Physics* 1992; **98**:231–253.
70. Mallad R, Sethian JA, Vemuri BC. A fast level set based algorithm for topology-independent shape modeling. *Journal Mathematical Imaging and Vision* 1996; **6**(2/3):269–290.
71. Adalsteinsson D, Sethian JA. The fast construction of extension velocities in level set methods. *Journal of Computational Physics* 1999; **148**(1):2–22.
72. Rodrigues H, Guedes JM, Bendsøe M. Hierarchical optimization of material and structure. *Structural and Multidisciplinary Optimization* 2002; **24**:1–10.
73. Wang SY, Tai K, Wang MY. An enhanced genetic algorithm for structural topology optimization. *International Journal for Numerical Methods in Engineering* 2005, in press.
74. Schaback R. Error estimates and condition numbers for radial basis function interpolation. *Advances in Computational Mathematics* 1995; **3**:251–264.
75. Michell AGM. The limits of economy of material in frame-structures. *Philosophical Magazine* 1904; **8**(6):589–597.

